Supporting Information

Solvent-Free Single-ion Conducting Polymer Electrolyte for Lithium-Metal Batteries Synthesized Via a Unique Donor-Acceptor Copolymerization

Yunfan Shao[1], Fannie Alloin[1,4,*], Dominic Bresser[2,3,*], Cristina Iojoiu[1,*]

[1] *Univ. Grenoble Alpes, Univ. Savoie Mont Blanc, CNRS, Grenoble INP, LEPMI, 38000 Grenoble, France*

[2] *Helmholtz Institute Ulm (HIU), 89081 Ulm, Germany*

[3] *Karlsruhe Institute of Technology (KIT), 76131 Karlsruhe, Germany*

[4] *Réseau sur le Stockage Electrochimique de l'Energie (RS2E), CNRS, FR3459, 80 039 Amiens Cedex, France*

***Corresponding authors:**

cristina.iojoiu@grenoble-inp.fr ; dominic.bresser@kit.edu ; fannie.alloin@grenoble-inp.fr

Keywords: polymer; electrolyte; single-ion; lithium metal; battery

1. Experimental

1.1 Materials

Poly(ethylene glycol) monomethyl ether (mPEG, Mw=1000 g mol^{-1}) was purchased from TCI. Maleic anhydride (MA), 4-fluorobenzenesulfonyl chloride, sodium hydride, lithium hydride and 4-hydroxyl butyl vinyl ether were purchased from Sigma-Aldrich. Trifluoromethanesulfonamide was purchased from Fluorochem. The photo initiator Lucirin lr 8893 was purchased from BASF. All the chemicals were used without purification.

Carbon-coated Al foil was purchased form MSE supplies, having a thickness of 16 µm (with 1 µm of carbon coating). The LFP powder was purchased from MTI corp. PVdF (Solef® 6020) was from Solvay S.A. The carbon black powder (Super C 65) was from TIMCAL.

1.2 Synthesis of lithium ((trifluoromethyl)sulfonyl) ((4-(4-(vinyloxy) butoxy) phenyl) sulfonyl) amide (PTFSIVE)

5 g 4-fluorobenzenesulfonyl chloride, 4.22 g trifluoromethanesulfonamide and 20 mL anhydrous dichloromethane were added to a three-neck flask under argon gas protectionin an ice bath. 5.72 g triethylamine was introduced via a dropping funnel. The reaction was then kept at room temperature for 10 h to yield a yellowish solution. After reaction, the solution was washed with DI water to remove the excess of trifluoromethanesulfonamide. Dichloromethane was removed by rotary evaporation. The product was dissolved again in 15 mL anhydrous THF and 1.5 g NaOH powder was added and stirred at ambient temperature overnight. The excess of NaOH was removed by filtration and THF was evaporated to yield the intermediate product, sodium ((4-fluorophenyl)sulfonyl)((trifluoromethyl)sulfonyl)amide.

To yield the final product, 1.5 g of 4-hydroxybutyl vinyl ether was dissolved in 10 mL of dry diglyme under argon. 328 mg NaH was introduced at 60 °C and stirred for 30 min to be fully dispersed. Then, 3 g of the intermediate product were added, and the temperature was elevated to 120 °C. The reaction was monitored by ^{19}F NMR, until the aromatic fluorine peak at about -109 ppm completely disappeared. After the reaction the diglyme was evaporated and the solid was dispersed in acetonitrile and filtered to remove the insoluble part. The solution was then mixed with 50% (v/v) DI water and passed through an amberlite IRC120 ion exchange column. The

acetonitrile was removed by evaporation and the DI water was removed by freeze drying to yield PTFSIVE.

1.3 Synthesis of poly(ethylene glycol) methyl ether maleate (mPEGME)

10 g mPEG was dissolved in 20 mL anhydrous THF and then mixed with 0.98 g maleic anhydride and stirred for 15 min at 40 °C. Then, 79.5 mg LiH was added. After reacting overnight, the mixture was filtered and the THF was removed by rotary evaporation.

1.4 Synthesis of the mPEGME-PTFSIVE copolymer

In a Schlenk flask, 0.93 g PTFSIVE, 5 g mPEGME and 60 mg of the photoinitiator Lucirin lr 8893 was dissolved in 5 mL anhydrous THF. The mixture was degassed during three cycles of freeze-pump-thaw. Then the flask was subjected to UV irradiation (mercury lamp, 365 nm, 6.8 W) upon magnetic stirring for 3 h, The product was purified by dialysis with a regenerated cellulous tubing against DI water for two days. The water was then removed by freeze drying.

1.5. Membrane casting

In a typical process for 70% of SIPE, 210 mg of mPEGME-PTFSIVE copolymer was mixed with 90 mg of PVdF-HFP and dissolved in 5 mL of a DMSO and acetone mixture (50:50) and cast in a small Petri dish. The solvent was dried at 80 °C for 12 h and then under vacuum for 12 h.

1.6 Methods

^{1}H, ^{19}F, ^{7}Li NMR spectra were taken using a Bruker Avance III HD 400MHz NMR spectrometer and processed with the Bruker topspin software. The samples were prepared in DMSO-d_6 or D_2O solvents for obtaining the spectra.

^{7}Li NMR was taken with an internal reference of $LiSO_3CF_3$ in DMSO-d_6 to determine the lithium content. The insertion tube was calibrated with three solutions of $LiSO_3CF_3$ in acetone-d_6 with

different concentrations (1.2, 1.3 and 1.8 g L^{-1}) by integrating the Li signals. The SIPE sample (4.5 and 8.0 g L^{-1}) was dissolved with $LiSO_3CF_3$ and inserted with the same internal reference to take ^{7}NMR spectra. The ratio between the area of the fluorine peaks in the $LiSO_3CF_3$ solution (with known concentration) and an internal reference was used for a calibration of the spectra. The Li concentration of the copolymer samples was determined by linear extrapolation of the calibration data. The calibration curve is shown in Figure S1.

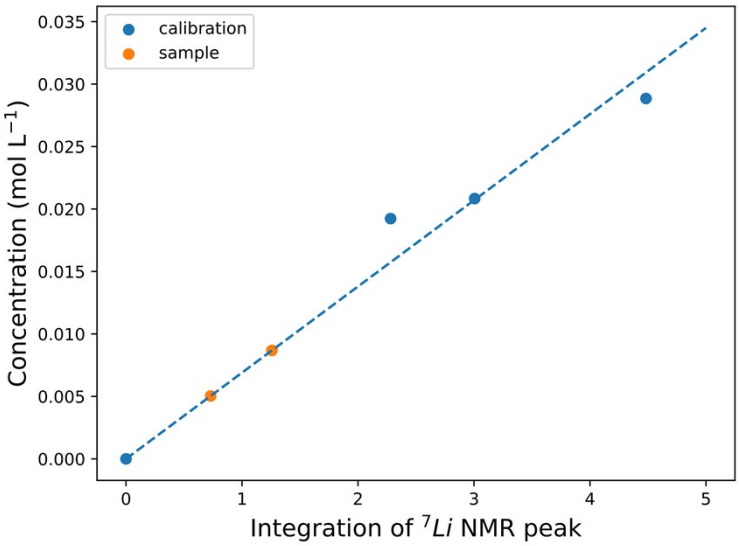

Figure S1*. Calibration curve for the determination of the Li concentration from ^{7}Li NMR data.*

SEC was measured using a Waters 515 HPLC pump and a 2414 RI detector with a Styragel HR GPC column in THF. The SEC was calibrated with standard polystyrene samples before use. SEL-LS was conducted with Agilent PLgel-Mixed-LS columns.

Atomic absorption spectroscopy (AAS) was conducted on a PerkinElmer PinAAcle 900 atomic absorption spectrometer. The device was calibrated with LiCl standards before use. The SIPE sample was prepared with an aqueous solution with a Li concentration of ~1 mg L^{-1}.

SEM images of the polymer membranes and LFP electrodes were recorded with a ZEISS Ultra 55 SEM equipped with an SE2 and in-lens detectors. For the ex situ studies, the Li|SIPE|Li cell were disassembled in a glovebox and inserted into the SEM with an airlock sample holder to avoid any contact with the ambient atmosphere. The SEM images were processed using the ImageJ software.[1]

X-ray tomography was at conducted with an RX-solutions Nano Computed Tomography System with a LaB_6 X-ray source (50 keV photon energy) and a CCD detector. The Li|SIPE|Li cells were disassembled and sliced in a glovebox and sealed in a plastic cylinder. The samples were scanned step-by-step with 6 pass and references of 1600 projections. The tomograph was reconstructed using the RX Solutions X-act software and the images were processed using the ImageJ software.

Differential scanning calorimetry (DSC) was conducted using a Mettler Toledo DSC1 STAR by increasing the temperature from RT to 125 °C then decreasing it to -100 °C and increasing it again to 125 °C with rate of 10 °C min^{-1} under nitrogen flow.

Thermogravimetric analysis (TGA) was conducted with a Mettler Toledo TGA1 STAR by increasing the temperature from RT to 500 °C with a rate of 10 °C min^{-1} under a nitrogen flow.

All the electrochemical tests were conducted using a Biologic VMP-300 potentiostat/galvanostat, and the data were processed using the Biologic EC-lab software.

Electrochemical impedance spectroscopy (EIS) was conducted in a frequency range from 7 MHz to 0.1 Hz. For each frequency, three measurements were performed, and the final spectra represent the average. The ionic conductivity was determined with the following equation:

$$\sigma = \frac{l}{R_B \cdot A} \#(1)$$

where l is the thickness of the electrolyte, R_B is the bulk resistance and A is the area of the electrode.

The Li^+ transference number was determined using symmetric Li|SIPE|Li cells at 80 °C using the Bruce-Vincent method:

$$T^{+}_{Li} = \frac{I_{ss}(\Delta V - I_0 R_0)}{I_0(\Delta V - I_{ss} R_{ss})} \#(2)$$

where ΔV is the bias voltage of the polarization, R_0, R_{ss} are the interfacial resistance of the initial and steady-state and I_0, I_{ss} are the current of the initial and steady-state.[2]

Cyclic voltammetry (CV) and linear sweep voltammetry (LSV) was conducted using Li|SIPE|stainless-steel (SS) cells at 80 °C. The scan rate was 0.2 mV s^{-1}. Current scan test was carried out with symmetric Li|SIPE|Li cells at 80 °C. The applied current ranged from 0 - 1.2 mA cm^{-2} with a scan rate of 0.1 μA s^{-1}.

1.7 Electrode preparation and cell assembly

The LFP active material, carbon black, PVdF and mPEGME-PTFSIVE copolymer were mixed with a mass ratio of 60:10:5:25. The mixture was dispersed in *N*-methyl-2-pyrrolidone (NMP) by using mortar and pestle to form a homogeneous slurry. The slurry was cast on carbon-coated aluminum foil serving as the current collector using a laboratory-scale doctor blade and dried at 60 °C for 24 h. Then the electrode was cut into discs of 12 mm diameter and calendared to reduce the porosity. The average LFP mass loading was around 1.5 mg cm^{-2}. LMB cells comprising LFP positive electrodes were assembled using CR2032-type coin cells in an argon filled glovebox by sandwiching the SIPE70 membranes between the LFP-based positive electrode and lithium metal. The coin cells were transferred to an isothermal chamber set to 80 °C and were allowed to rest for 6 h before any further testing.

2. Results and Discussion

2.1 NMR spectroscopy

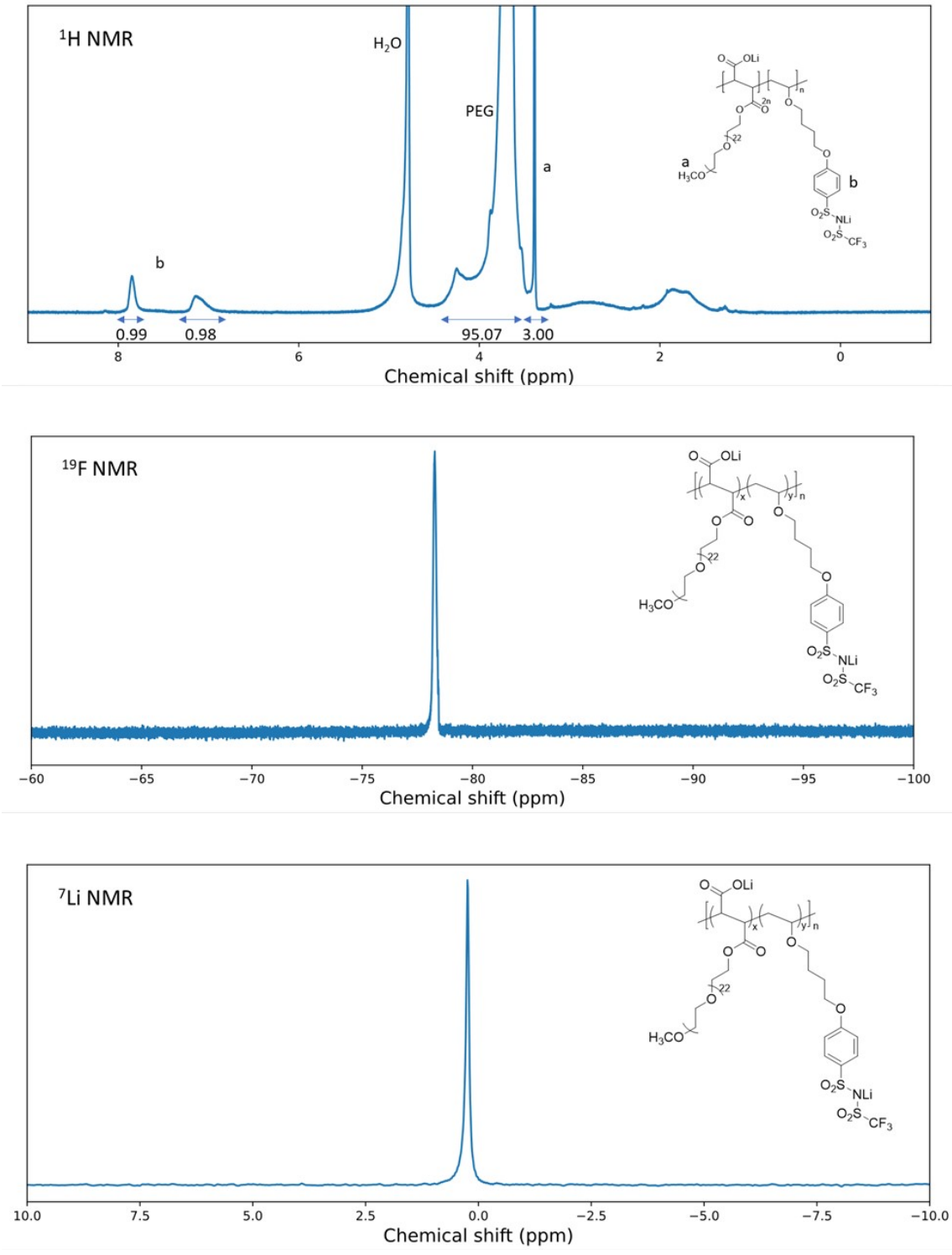

Figure S2. *^{1}H, ^{19}F and ^{7}Li NMR spectra of the mPEGME-PTFSIVE copolymer in D_2O.*

$$A{:}D = \frac{n_{mPEGME}}{n_{PTFSIVE}} = \frac{4H_{OCH3}}{3H_{Ar}} \# (3)$$

Where A:D is the ratio between the electron acceptor and donor moieties in the copolymer, which can be calculated by the NMR integrated peak ratio of the methoxy terminal group in the mPEGME monomer and the aromatic rings in the PTFSIVE monomer.

2.2 IR spectra of the mPEGME-PTFSIVE copolymer

The chemical structure of the polymer was moreover analyzed by Fourier-transform infrared (FTIR) spectroscopy in attenuated total reflectance (ATR). The absorption spectrum from 3500 to 450 cm^{-1} is shown in Figure S3. The vibration of the PEG side chain is very apparent as stretching of the C-H and C-O bonds at 2865 and 1091 cm^{-1}, respectively. Other than the PEG signals, the stretching of the ester function, specifically C=O, appears at 1735 cm^{-1}; aromatic C=C bond stretching and bending can be found at 1597 and 843 cm^{-1}. For the TFSI group, the vibrations modes are more weak and complicated, by referring the spectra from literature[3], the stretching of the S-N-S and bending of C-F, S-N-S, S=O can be recognized in the magnified spectrum between 800-450 cm^{-1} (Figure S4). All the expected functional groups were observed in the IR spectrum, which correspond to the proposed polymer structure.

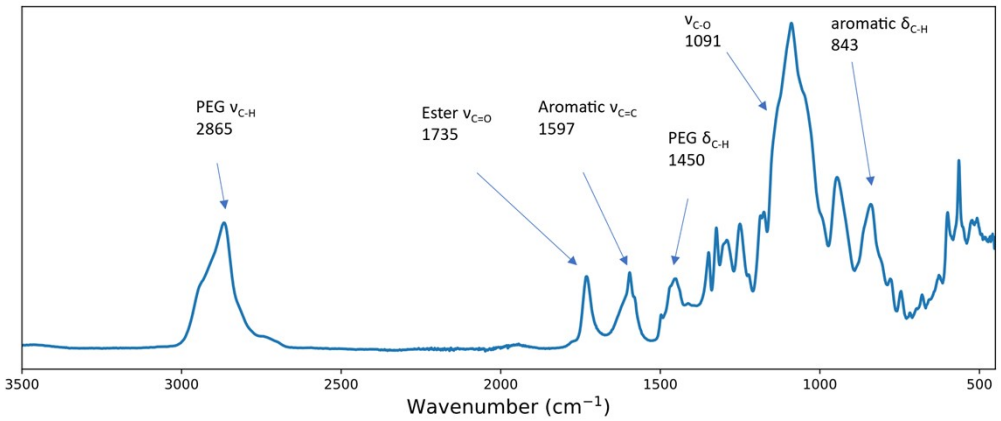

Figure S3. *ATR-FTIR absorption spectrum of the mPEGME-PTFSIVE copolymer.*

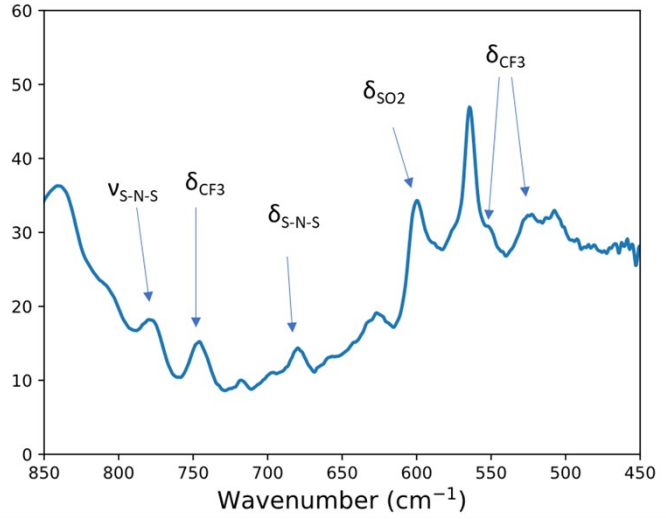

Figure S4. *ATR-FTIR spectrum of mPEGME-PTFSIV, magnified from 850-450 cm^{-1}.*

2.3 Model molecules

Common aliphatic vinyl ether and maleate were chosen to exemplify the donor-acceptor copolymerizations. Butyl vinyl ether (BVE) and diethyl maleate (DEM) were polymerized with the same protocol described before. The product was purified by dissolution in ethanol and precipitation in water. After drying under vacuum, a white polymer was obtained. The reaction is shown in Figure S5.

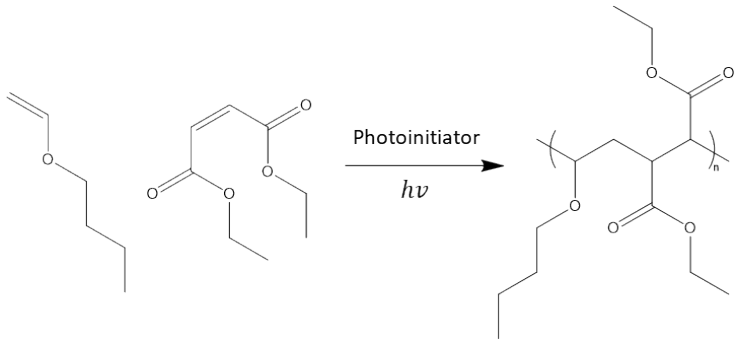

Figure S5. *Synthesis of BVE-DEM copolymer.*

A ^{1}H NMR spectrum, shown in Figure S6, was taken to examine the A: D ratio of this BVE-DEM copolymer. By comparing the spectra of the monomers, although the broad peaks are overlapping which renders the integration challenging, the specific peaks could be clearly assigned. The peak

at the lower chemical shift of 0.89 ppm is the signal of CH_3 at the end of the BVE, which integrated as 3. Then the peak at the highest chemical shift of 4.10 ppm corresponds to the CH_2 close to carboxyl with an integration of 4.45. These two peaks are well separated from all the other broad peaks that are easy to recognize and integrate. Thus, the A:D ratio of the monomers can be determined as 1: 1.11, which is close to one and aligned with most of the cases for the donor-acceptor polymerization.

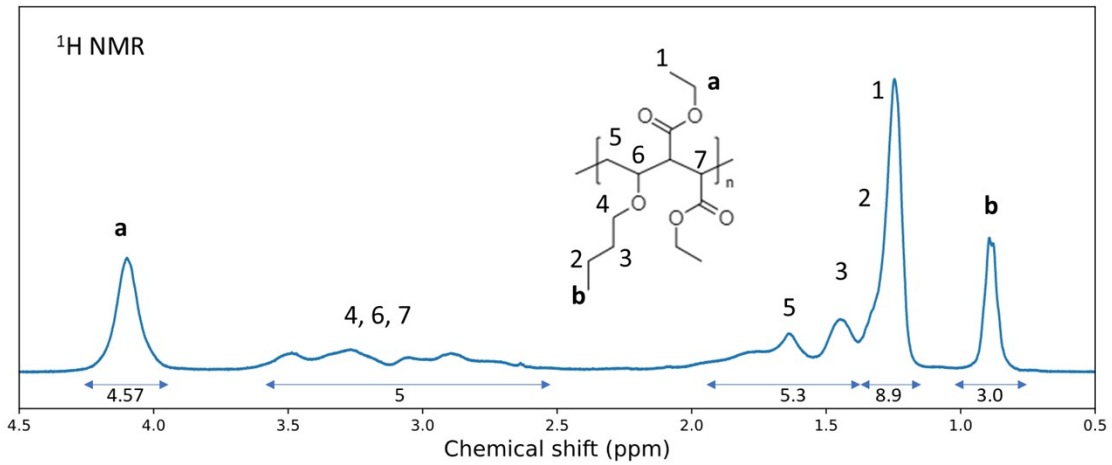

Figure S6. *^{1}H NMR spectrum of the BVE-DEM copolymer in $CDCl_3$.*

Ionic PTFSIVE was mixed with diethyl maleate and polymerized (Figure S7) with the photoinitiator under UV irradiation. The product was purified by dialysis. Similarly, the product showed an A:D ratio of 2, again regardless of the feeding ratio of the two monomers. As shown in the ^{1}H NMR spectrum (Figure S8), for the PTFSIVE-DEM copolymer, CH_3 from DEM (a) and the aromatic protons from PTFSIVE (b) were integrated, revealing 6 and 2.14, which could be converted to DEM: PTFSIVE with a ratio of x:y = 2:1.07. The DEM-PTFSIVE copolymer confirms the formation of a copolymer with an unusual ratio between electron acceptor and donor, i.e., A:D = 2. Taking into account that mPEGME-PTFSIVE and DEM-PTFSIVE copolymers involve the ionic monomer PTFSIVE, which led to such structure, it can be supposed that the special acceptor-donor ratio is linked to the presence of the ionic monomer.

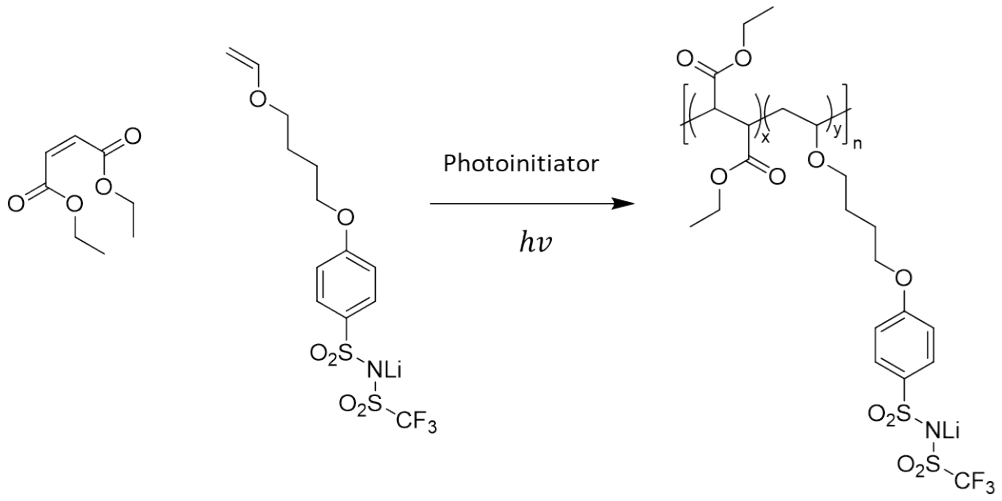

Figure S7. *Depiction of the synthesis of the PTFSIVE-DEM copolymer.*

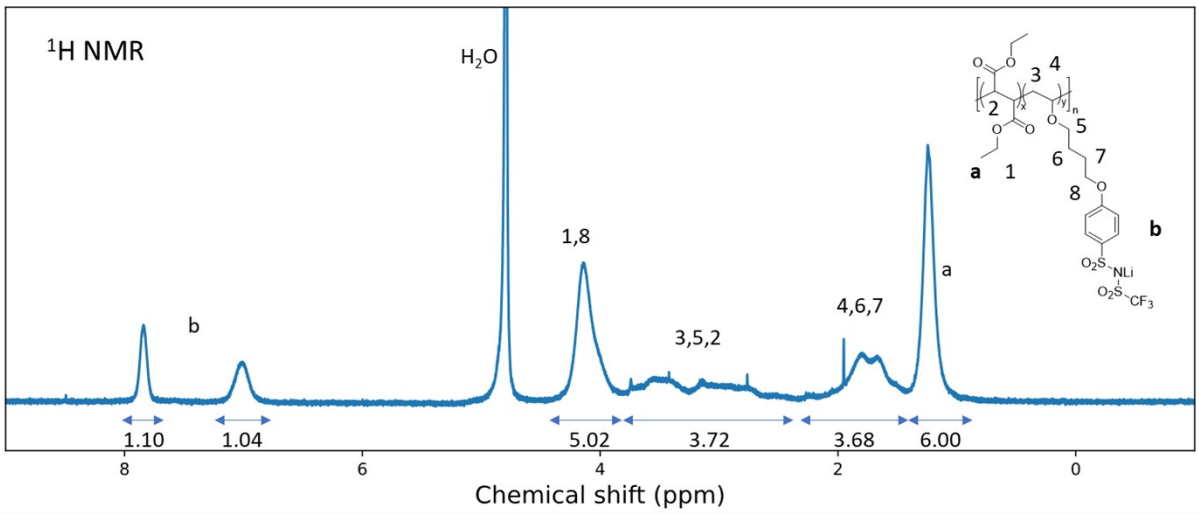

Figure S8. *^{1}H NMR spectrum of the DEM-PTFSIVE copolymer in $CDCl_3$.*

2.4 Porosity and morphology

The porosity can be calculated from the density of the membrane. The weight of a piece of membrane was measured in argon atmosphere as well as after immersion in heptane, the last could fill the porosity but not swell the membrane. After removing the buoyancy of the heptane, the density of the membrane can be calculated with the following equation:

$$\rho = \frac{A}{A-B}(\rho_0 - \rho_L) + \rho_L \#(4)$$

where A is the sample weight in air, B is the sample weight in heptane, ρ_0 and ρ_L are the densities of heptane and argon, respectively. The density of the SIPE70 membrane determined with this method was 1.50 g cm^{-3}, while the apparent density calculated with geometric dimensions was 1.22 g cm^{-3}, which is between the density of PVdF-HFP with around 1.8 g cm^{-3} and PEO with around 1.2 g cm^{-3}. The density of the SIPE70 membrane was accordingly within the expectation. The porosity of the SIPE70 membrane could be determined by:

$$porosity = 1 - \frac{V_{real}}{V_{geometric}} = 1 - \frac{\rho_{geometric}}{\rho_{real}} \#(5)$$

Thus, the porosity of the SIPE70 membrane was calculated to be 19%, which seems coherent with the SEM images.

2.5 Li^+ transference number

The electrolyte and interphase contributions in Figure 2 were determined with the help of an electric circuit model, as depicted in Figure S9. In the circuit, R1, R2 and R3 represent the resistance of the experimental setup, the bulk resistance of the electrolyte and the interphase resistance, respectively. Q2 and Q3 are the constant phase elements of the electrolyte and interphase, respectively. The fitting results are given in Table S1.

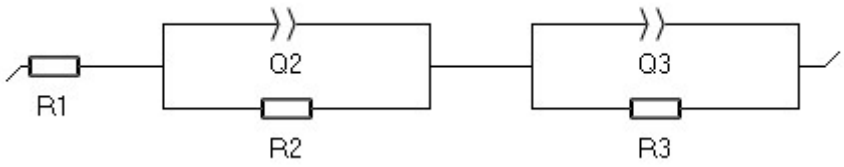

Figure S9. *Equivalent circuit model for the Li|SIPE|Li cell system.*

Table S1. EIS fitting results for the Li|SIPE70|Li cells before and after polarization.

	R1 (Ω)	R2 (Ω)	R3 (Ω)	Q2 (F $s^{-0.2}$)	Q3 (F $s^{-0.2}$)
Before	38	705	85	10.3×10^{-9}	1.4×10^{-6}
After	38	706	85	10.3×10^{-9}	1.4×10^{-6}

2.6 Linear sweep and cyclic voltammetries

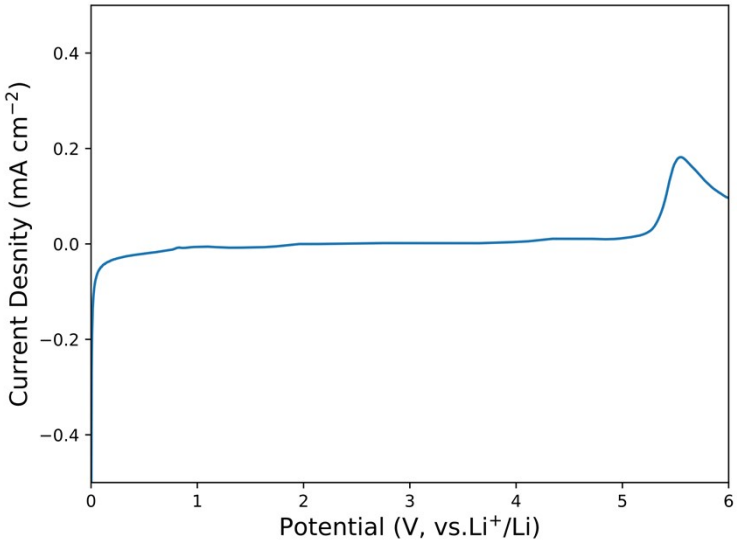

Figure S10. *LSV trace of the Li|SIPE70|SS cells, from 0-6 V vs. Li^+/Li.*

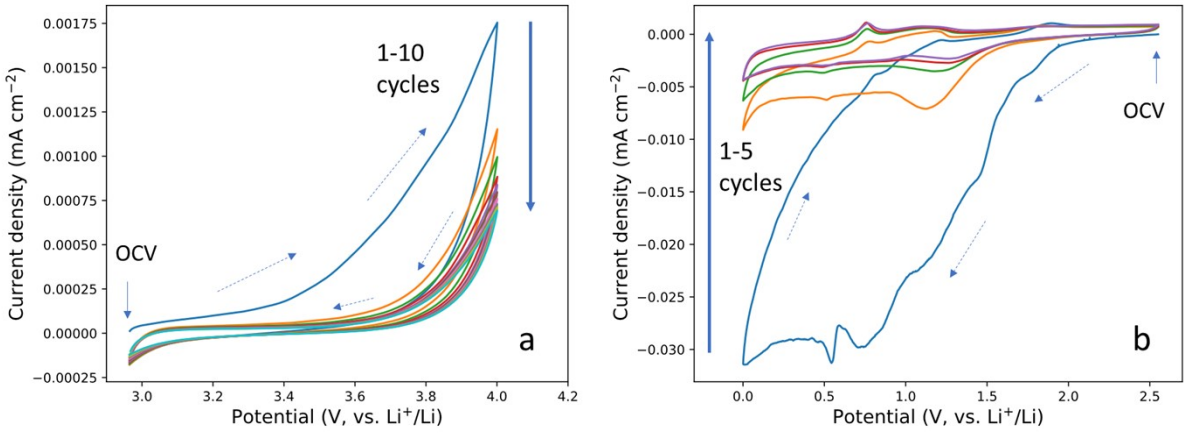

Figure S11. *CV traces of the Li|SIPE70|SS cells: (a) from OCV to 4.0 V; (b) from 0 V to OCV.*

To investigate side reactions before the lithium plating, cathodic scans were conducted on cells between OCV and 0 V. The first cycle showed a strong reaction between 1.5 V and 0 V vs. Li^+/Li, which could be associated with the reduction of the electrolyte and the formation of a passivation layer, as indicated by a decreasing current in the following cycles. Additionally, a pair of small peaks could be observed in the anodic scan at 0.5 and 0.8 V vs. Li^+/Li, which appear largely reversible, and have been assigned the de-/lithiation of oxidic surface species on the working electrode [4].

2.7 Li stripping/plating experiments and determination of the critical current density

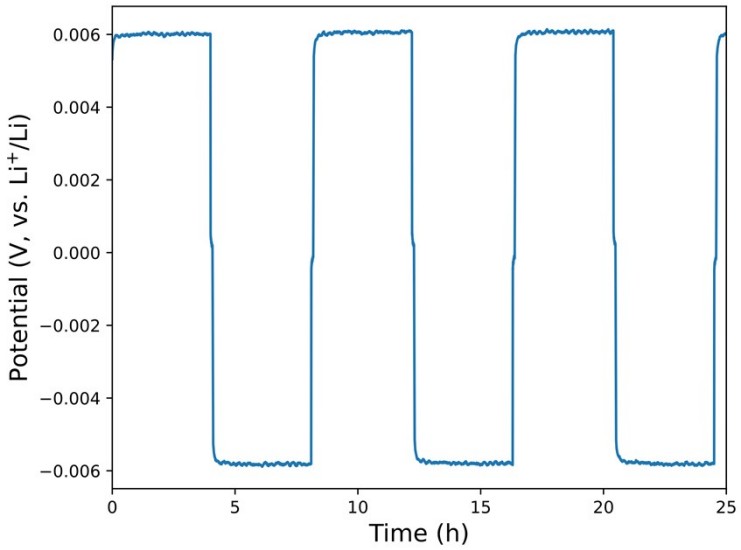

Figure S12. *Magnification of the lithium stripping/plating cycles from 0-25 h with a current density of 10 µA cm^{-2}.*

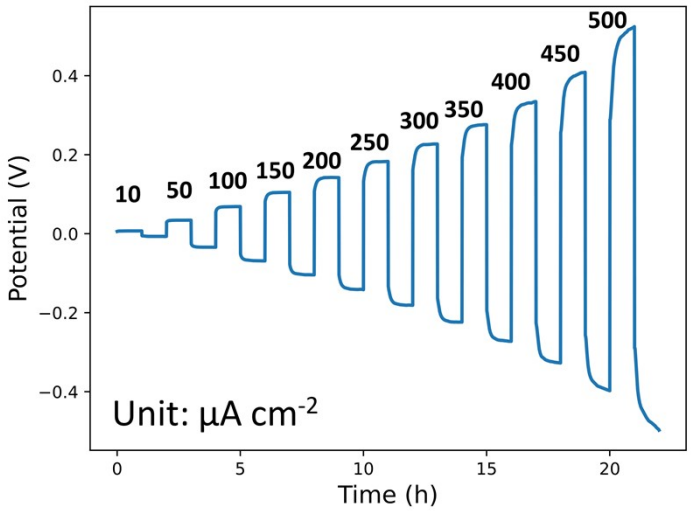

Figure S13. *Lithium plating/stripping experiment with an increasing current density.*

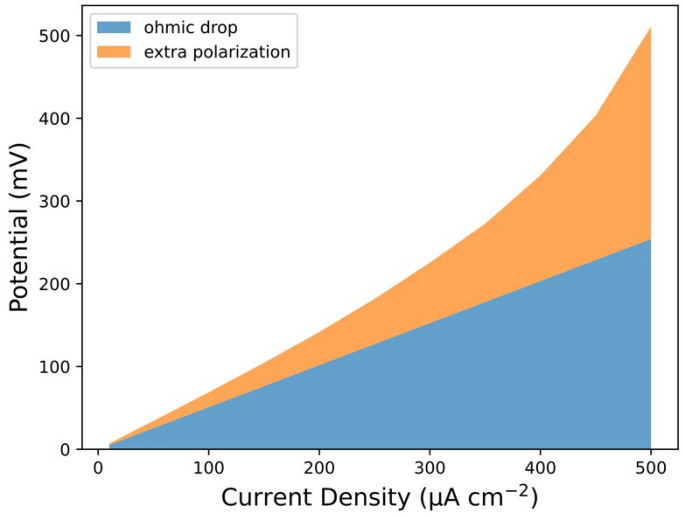

Figure S14. *The extra polarization during the Li plating/stripping experiments as a function of the applied current density.*

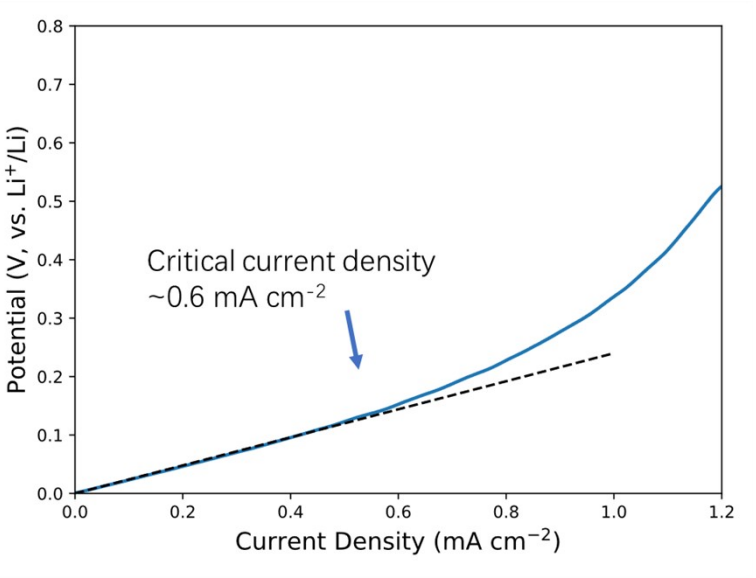

Figure S15. *Current density scan of a Li|SIPE70|Li with a scan rate of 0.1 μA s^{-1}.*

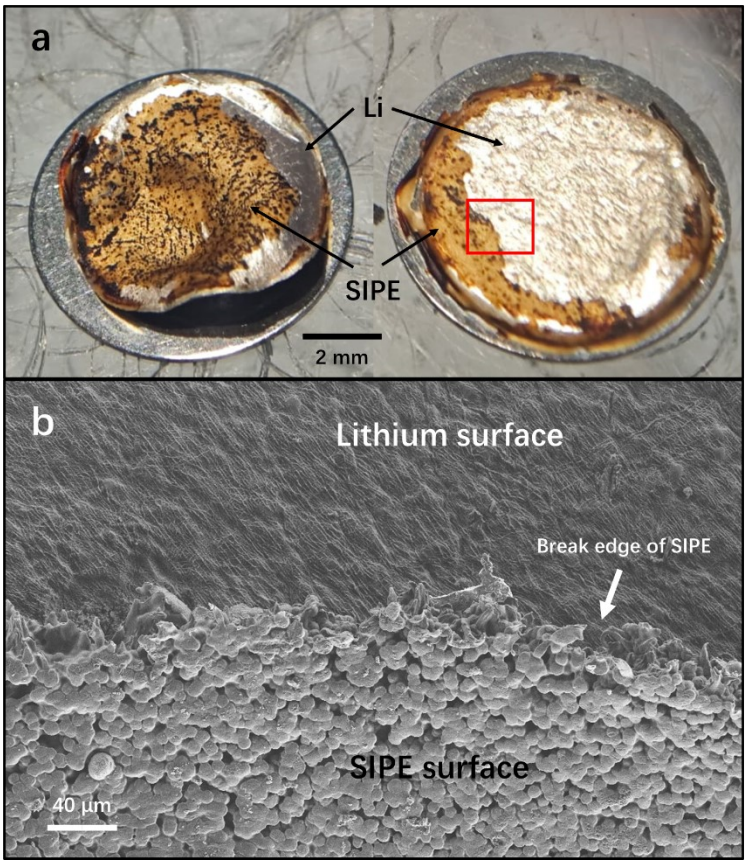

Figure S16. *(a) Photo of a disassembled Li|SIPE|Li cell after lithium stripping/plating for 148 h at 100 µA cm^{-2}. The part in the red box was examined by SEM. (b) SEM image of the lithium surface and the SIPE in the Li|SIPE|Li cell after lithium stripping/plating for 148 h at 100 µA cm^{-2}.*

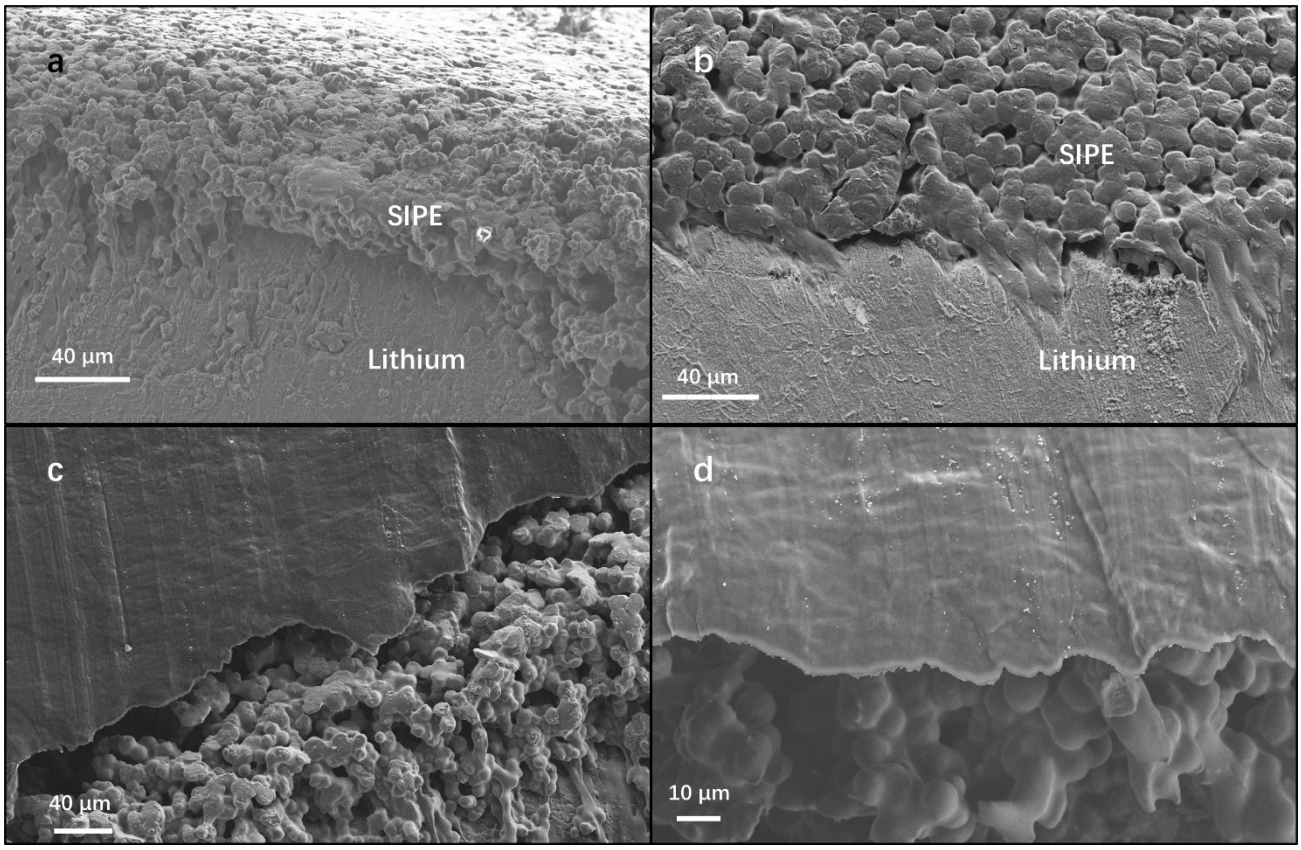

Figure S17. *Cross-sectional SEM images of SIPE|Li interfaces in the Li|SIPE|Li cell after lithium stripping/plating; (a-d) sample after cycling for (a,b) 148 h and (c,d) 200 h at current density of 100 µA cm^{-2}.*

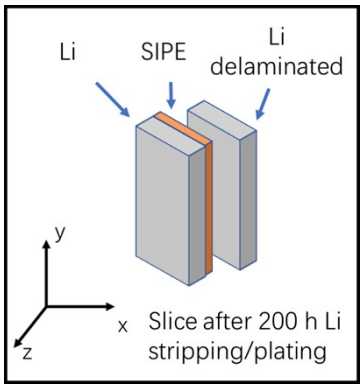

Figure S18. *Schematic illustration of the X-ray tomography samples.*

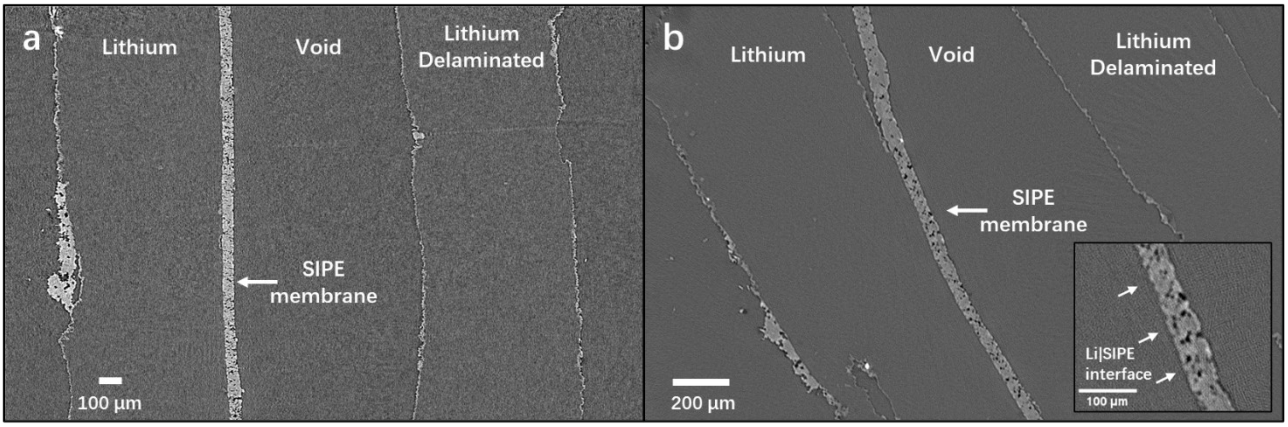

Figure S19. *X-ray tomograph of the Li|SIPE|Li cell after lithium stripping/plating for 200 h at a current density of 100 µA cm^{-2}. (a) Slice in Z axis; (b) Slice in Y axis. The inset is the magnified regions close to SIPE|Li interface.*

2.8 Li|SIPE|LFP cells

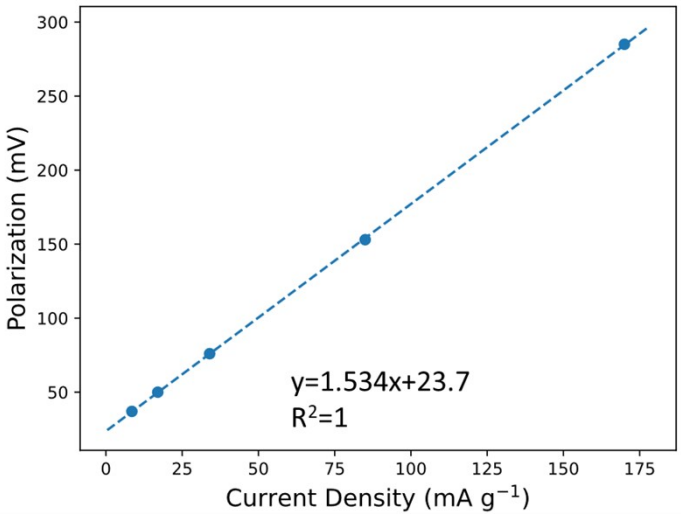

Figure S20. *Polarization vs. current density of the Li|SIPE|LFP cells from the C rate test.*

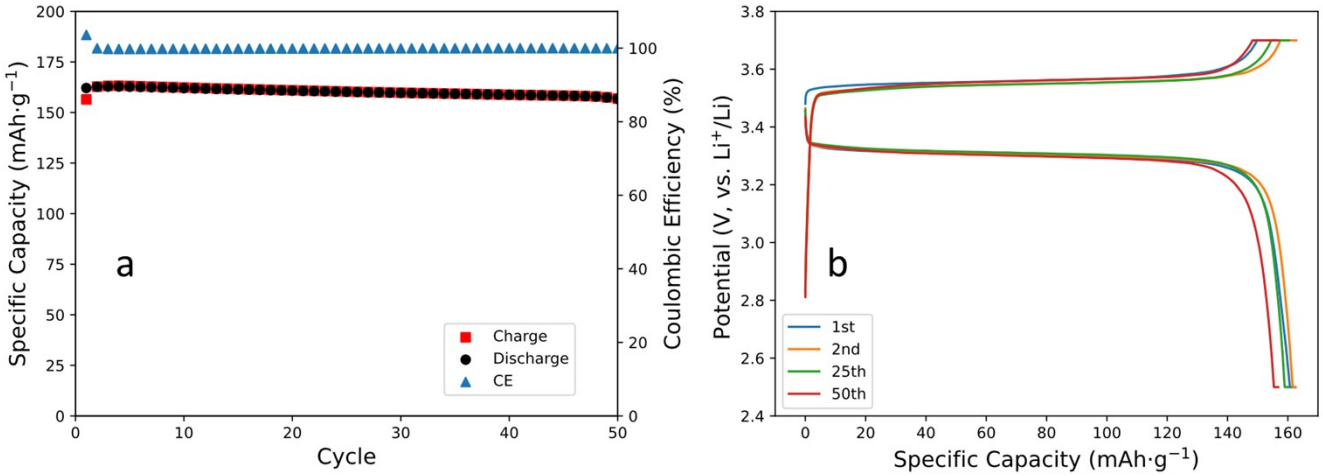

Figure S21. *Li|SIPE70|LFP cells with mPEGME-PTFSIVE as the electrolyte at 40 °C: (a) plot of the capacity and Coulombic efficiency vs. the cycle number and (b) selected dis-/charge profiles.*

2.9 Comparison with state-of-art solvent-free SIPEs

The glass transition temperature, conductivity (at a certain temperature), and the lithium transference number of high-performance, solvent-free SIPEs reported in the literature are summarized in Table S2. These properties mainly represent the charge transport behavior of SIPEs. SIPE100 and SIPE70 show comparable properties as the best results reported so far.

Table S2. Comparison of the solvent-free SIPEs.

Electrolyte	**T_g (°C)**	**Conductivity (S cm^{-1})**	**Testing temperature (°C)**	**T_{Li^+}**	**Ref.**
PEO-PSLiTFSI	160 (PSLiTFSI)	3.8×10^{-4}	90	0.95	[5]
PS-b-P(MALi-co-POEGMA)	-70	10^{-8}	20	~1	[6]
LiPSsTFSI / PEO	44.3	1.35×10^{-4}	90	0.91	[7]
LiBC-1	-61	2.3×10^{-6}	25	0.83	[8]
LiMTFSI-PEO-LiMTFSI	95 (LiMTFSI)	10^{-4}	70	0.91	[9]
P(STFSILi)-PEO-P(STFSILi)	-	1.3×10^{-5}	60	0.85	[10]
PEOMA-TFSI$^-$Li$^+$	-17	4.73×10^{-5}	90	0.99	[11]
LiPBPAB / PEO	-	1.7×10^{-4}	60	0.96	[12]
LiPCSI / PEO	-4.5	7.3×10^{-5}	60	0.84	[13]
poly[TMC$_n$-b-(LiM$_m$-r-PEGM$_k$)]	-49, -16	4×10^{-6}	70	0.91	[14]
PTFSIVE-mPEGME	-55	5.01×10^{-5}	90	0.9	This work

Table S3. Comparison of selected solid-state LFP battery cells reported in the literature.

Name of electrolyte	T (°C)	Specific capacity (mAh g^{-1})	Cycle life (retention)	Ref.
PDMS−poly(STF−Li^+−r−PEGMA)$_{20}$	65	107 100th cycle at C/10	100 at C/10 (81.5)	[8]
LiBC-1	70	130 at C/15	100	[8]
poly[TMC_n-b-(LiM_m-r-$PEGM_k$)]	70	145 at C/20	>50 at C/20	[14]
LIPBPAB / PEO	80-50	147 1st cycle at C/25	>90	[12]
LiMTFSI-PEO- LiMTFSI	70	153 at C/10	300 at C/2 (77.8%)	[9]
LiPCSI/PEO	60	141 1st cycle at C/10	80 at C/10 (85.1%)	[13]
PTFSIVE-mEPGME	80	153 4th cycle at C/10	100(86%)	This work
	40	151 26th cycle at C/10	70(93%)	

The comparison with previously reported results shows that the SIPE reported herein provides the best capacity when employed in Li|SIPE|LFP cells at high temperatures together with the highest capacity retention after 100 cycles. Additionally, this is the only work that showed battery tests at 40 °C which also provided very good performance, even comparable to the results reported in previous studies and conducted at higher temperatures (Table S3).

References

1 C. A. Schneider, W. S. Rasband and K. W. Eliceiri, *Nat Methods*, 2012, 9, 671–675.
2 J. Evans, C. A. Vincent and P. G. Bruce, *Polymer*, 1987, 28, 2324–2328.
3 A. Narita, W. Shibayama and H. Ohno, *J. Mater. Chem.*, 2006, 16, 1475.
4 M. Wetjen, G.-T. Kim, M. Joost, M. Winter and S. Passerini, *Electrochimica Acta*, 2013, 87, 779–787.
5 S. Inceoglu, A. A. Rojas, D. Devaux, X. C. Chen, G. M. Stone and N. P. Balsara, *ACS Macro Lett.*, 2014, 3, 510–514.
6 J. Rolland, E. Poggi, A. Vlad and J.-F. Gohy, *Polymer*, 2015, 68, 344–352.
7 Q. Ma, H. Zhang, C. Zhou, L. Zheng, P. Cheng, J. Nie, W. Feng, Y.-S. Hu, H. Li, X. Huang, L. Chen, M. Armand and Z. Zhou, *Angew. Chem. Int. Ed.*, 2016, 55, 2521–2525.
8 L. Porcarelli, A. S. Shaplov, M. Salsamendi, J. R. Nair, Y. S. Vygodskii, D. Mecerreyes and C. Gerbaldi, *ACS Appl. Mater. Interfaces*, 2016, 8, 10350–10359.
9 L. Porcarelli, M. A. Aboudzadeh, L. Rubatat, J. R. Nair, A. S. Shaplov, C. Gerbaldi and D. Mecerreyes, *Journal of Power Sources*, 2017, 364, 191–199.
10 R. Bouchet, S. Maria, R. Meziane, A. Aboulaich, L. Lienafa, J.-P. Bonnet, T. N. T. Phan, D. Bertin, D. Gigmes, D. Devaux, R. Denoyel and M. Armand, *Nature Mater*, 2013, 12, 452–457.
11 S. Li, A. I. Mohamed, V. Pande, H. Wang, J. Cuthbert, X. Pan, H. He, Z. Wang, V. Viswanathan, J. F. Whitacre and K. Matyjaszewski, *ACS Energy Lett.*, 2018, 3, 20–27.
12 Y. Zhang, W. Cai, R. Rohan, M. Pan, Y. Liu, X. Liu, C. Li, Y. Sun and H. Cheng, *Journal of Power Sources*, 2016, 306, 152–161.
13 H. Yuan, J. Luan, Z. Yang, J. Zhang, Y. Wu, Z. Lu and H. Liu, *ACS Appl. Mater. Interfaces*, 2020, 12, 7249–7256.
14 G. Lingua, P. Grysan, P. S. Vlasov, P. Verge, A. S. Shaplov and C. Gerbaldi, *Macromolecules*, 2021, 54, 6911–6924.